Journal of Testing and Evaluation

doi:10.1520/JTE20230747 / Vol. 52 / No. 4 / 2024 / available online at go.astm.org/pubs

Paul Sukpe,[1,2] Rade Vignjevic,[3] Kevin Hughes,[3] and Rob Kulka[2]

Experimental Investigation of Crack Tip Constraint Effects on Fracture Assessment of API 5L X65 Steel Grade for Low-Temperature Applications (–120°C)

Manuscript received November 30, 2023; accepted for publication February 12, 2024; published online May 29, 2024. Issue published July 1, 2024.

[1] Brunel University London, Kingston Ln., London, Uxbridge UB8 3PH, UK (Corresponding author), e-mail: paulsukpe@gmail.com, https://orcid.org/0000-0001-9168-9672

[2] The Welding Institute Ltd./National Structural Integrity Research Centre, Granta Park, Great Abington, Cambridge, CB21 6AL, UK

[3] Brunel University London, Kingston Ln., London, Uxbridge UB8 3PH, UK

Reference

P. Sukpe, R. Vignjevic, K. Hughes, and R. Kulka, "Experimental Investigation of Crack Tip Constraint Effects on Fracture Assessment of API 5L X65 Steel Grade for Low-Temperature Applications (–120°C)," *Journal of Testing and Evaluation* 52, no. 4 (July/August 2024): 2083–2104. https://doi.org/10.1520/JTE20230747

ABSTRACT

Crack tip constraint is a significant issue in engineering components' design and repair decisions. The main reason is that fracture assessment procedures, such as BS 7910, rely on lower-bound fracture toughness test data from deeply cracked bend specimens. This can generate stress states under various loading conditions with an appropriate crack tip stress triaxiality for metallic structures. Many real components (e.g., oil and gas pipelines) have small in-plane (shallow cracks) and out-of-plane (thin-wall thickness) dimensions that can cause a reduction in crack tip constraint to a considerable amount, thereby increasing the fracture toughness. As such, the structural assessment of low-constraint structural components using fracture toughness data obtained from deeply notched specimens may be safe but overly conservative, resulting in unnecessary repair shutdowns and costs. Consequently, relating fracture toughness values determined from laboratory specimens to real structural components becomes an issue in structural integrity assessments based on the two-parameter fracture mechanics methodology. This study investigates the applicability of the constraint-based failure assessment diagram (FAD) approach for the evaluation of cracked pin-loaded single-edge notched tension and three-point single-edge notched bend specimens at low (–120°C) and room temperatures. The analyses reveal that the experimentally measured toughness values, J_0, depend on the crack sizes for the considered specimen geometries ($a/W = 0.1$, 0.3, 0.5). The results show the benefits of using constraint-modified FAD approach for the assessment of shallow cracks. Therefore, the enhanced toughness associated with constraint reduction indicated an increased margin and allows realistic design and repair decision-making that can help prevent catastrophic failures.

Keywords

brittle fracture, defects, integrity assessment, low temperature, shallow crack

Nomenclature

a = crack length
a_0 = initial crack length
B = thickness of specimen
E = Young's modulus in-plane stress
E' = Young's modulus in-plane strain
J = J-integral
J_{el} = elastic component of J
J_{pl} = plastic component of J
K = stress intensity factor
K_I = Mode I stress intensity factor
K_{mat} = material fracture toughness measured by stress intensity factor
K_r = fracture ratio of applied K and K_{mat}
L_r = load ratio
n = strain-hardening exponent
P = applied load
P_b = primary bending stress
P_L = limit load
P_m = primary membrane stress
Q = elastic-plastic constraint parameter
T = elastic constraint parameter/T stress
T-L = transverse longitudinal
W = width of specimen
V_{p1} and V_{p2} = plastic parts of the clip gage displacements of the knife heights of Z_1 and Z_2
Z_1 and Z_2 = clip gage displacements of the knife heights
α = Ramberg-Osgood fitting parameter
β = normalized structural constraint parameter
δ = crack tip opening displacement
η_p = dimensionless function of geometry
ν = Poisson's ratio
σ = stress
σ_0 = normalizing or yield stress
$\sigma_{0.2}$ = 0.2 % proof stress on true stress-strain curve
σ_{ref} = reference stress
σ_Y = yield stress

Introduction

The development of Arctic oil and gas infrastructure requires fixed offshore structures and pipelines capable of operating safely at low temperatures and typically manufactured from steel. This is due to its relatively low cost, ease of fabrication, and high strength and fracture resistance properties. However, the Arctic environment is hazardous from a structural integrity standpoint, as steel increases susceptibility to brittle fracture at low temperatures that can result in catastrophic failure, irreparable damage, and potential loss of life.[1]

Therefore, an appropriate material toughness criterion is needed to ensure high-strength steels with adequate fracture resistance at low temperatures are used in Arctic constructions. In the past decade, significant efforts have been made in the development of fitness-for-service procedures applicable to defect assessments and life-extension programs of critical engineering components. These methodologies, called engineering critical assessment (ECA) procedures, provide a concise framework to relate crack size with applied loading using failure assessment diagrams (FADs). These approaches rely on the use of lower-bound fracture toughness data determined from deeply notched bend (SENB) and compact tension (CT) specimens to guarantee representative levels of stress triaxiality, which drive the fracture process.[2,3] A single geometry-independent failure locus provides a highly effective but conservative acceptance criterion for cracked structural components under such conditions. Several assessment methodologies are now well established, e.g., BS 7910, *Guide to Methods for Assessing the Acceptability of Flaws in Metallic Structures*,[4] R6, *British Energy Generation Limited: Assessment of the Integrity of Structures Containing Defects*,[5] and API 579/ASME FFS-1, *Fitness-for-Service*,[6] among others, which are based upon the FAD concept and are widely employed to analyze structural defects.

However, the most common defects in pipelines are surface cracks that have low levels of crack tip stress triaxiality, which significantly differs from the stress states present in deeply notched specimens. ECA procedures applicable to offshore pipelines rely on the direct application of crack growth resistance curves (*R*-curves) determined using small laboratory specimens to define acceptable defect sizes for conservative assessments. Therefore, the applicability of experimentally determined fracture toughness data for structural steel piping components is of high importance for accurate predictions of in-service residual strength and remaining life to reduce maintenance downtime and costs.[7]

At present, BS 7910 does not offer guidance for refinement/enhancement of estimation of toughness for shallow cracks in thin-wall structures, apart from testing the exact component geometry which may not always be practicable or appropriate. To quote BS 7910 Clause 7,[4] "it is common practice to use fracture toughness specimens that are representative of the thickness of the component being assessed." This paper focuses on evaluating the effects and influence of constraint on material fracture resistance for API 5L X65 high-strength steel.

Experimentally determined fracture toughness/resistance curves typically exhibit a significant dependency on specimen geometry, crack size (characterized by the a/W ratio), and loading mode (bending versus tension).[8] For the same material, high-constraint configurations, such as deeply notched SENB and CT specimens produce low fracture toughness. In contrast, shallow-notched SENB and predominantly tension-loaded designs (single-edge notched tension [SENT]) are associated with higher toughness values for similar amounts of crack extension.[9,10]

The primary motivation to use SENT fracture specimens in defect assessment procedures for structural offshore steel pipes is the similarity in crack tip stress and strain fields driving the fracture process for both crack configurations, as previously reported by Nyhus et al.[11–13] Xu et al.[14,15] also investigated the effects of constraint on ductile fracture toughness for clamped SENT and deeply notched SENB fracture specimens. By correlating experimental results with ductile fracture behavior in circumferentially cracked pipes, the authors concluded that SENT and shallow-cracked SENB have crack tip constraint conditions similar to circumferentially cracked pipes. Cravero and Ruggieri[8] generated a range of *J*-resistance curves for pin-loaded and clamped SENT specimens using the unloading compliance method. Their results provided further support for the development of standard test procedures for SENT specimens applicable in measuring crack growth resistance for pipelines.[16]

These previous investigations represent a significant milestone in engineering applications of SENT fracture specimens that relate directly to structural integrity assessments of pipelines. A common approach is comparing SENT configurations having varying crack depths against a standard, deeply cracked SENB specimen with $a/W = 0.5$. In these cases, the evolving levels of crack tip constraint with increased remote loading in the SENT specimens are closely related to the corresponding levels of stress triaxiality for a surface cracked pipe under predominantly tensile loading. However, a more systematic investigation of the toughness dependency as a function of constraint is required to assess the similarity between SENT and circumferentially surface cracked pipes. Nevertheless, the use of SENT specimens to characterize fracture resistance properties in steel pipelines has been effective in reducing overconservatism that arises when measuring fracture toughness using high-constraint specimens.[10,17,18]

Despite SENT specimens being routinely used in pipeline fracture testing, some difficulties are associated with test fixture and gripping conditions, low constraint conditions, and high loads required to propagate the crack. This raises concerns about the validity and accuracy of the measured fracture resistance curves. Often viewed as nonconventional and slightly more conservative, shallow-notched bend SENB testing configuration may become more attractive due to its simpler testing procedures and smaller loads required for crack propagation. Therefore, using smaller specimens that guarantee adequate levels of crack tip constraint to measure the material's fracture toughness represents an attractive alternative.[19]

As we extend our understanding of the fracture toughness of high-strength steels, especially in the context of shallow cracks and low temperatures, the existing literature has provided valuable insights into historical perspectives, normative references, and recent advances. However, a critical gap exists in the availability of comprehensive material test data for high-strength steels, particularly when subjected to the extreme temperature of −120°C. The novelty of the current research lies in its dedication to generating new and robust material test data specifically for API 5L X65 steel at −120°C. This extreme temperature is chosen deliberately to align with the operating conditions of critical infrastructure, such as oil and gas pipelines in harsh environments. The results obtained will contribute significantly to the understanding of how high-strength steels, under the influence of shallow cracks, perform in such challenging conditions. By linking the state-of-the-art literature review to the experimental data generated in this paper, we aim to bridge the gap between theoretical concepts and practical applications. The new material test data serve not only to augment our understanding of fracture toughness in high-strength steels but also to provide valuable inputs for the development of more accurate predictive models.

Motivated by these observations, this work investigates the applicability of the constraint-based FAD method in the assessment of cracked SENT and SENB specimens at low (−120°C) and room temperatures. The fracture tests were performed for three different crack configurations, $a_0/W = 0.1$, 0.3, and 0.5 (where a_0 is the initial crack length and W is the width of the specimen). As part of the constraint-modified FAD calculations, CrackWISE software[20] was used to derive the respective FADs. One of the objectives of this work was to improve and refine defect assessment procedures that include the effects of constraint variation on fracture toughness when assessing shallow cracks.

Experimental Testing and Procedures

Tensile and fracture toughness tests were performed on API 5L X65 steel. Mechanical properties and fracture toughness were determined at room (23°C) and low (−120°C) temperatures. The methods developed for the base metal should also be applicable to welds (with suitable corrections for the crack driving force applied as part of a defect tolerance analysis). This is generally true, as the behavior of welds is closely related to that of the base metal, and many of the same principles and techniques used in assessing the performance of base metal can also be applied to welds. However, it is important to note that the presence of a weld can introduce additional factors that may need to be considered when assessing its performance. For example, welding can result in residual stresses, which can increase the susceptibility of the material to fracture. In addition, the presence of a weld can create a region of altered microstructure that can affect the material's properties and behavior. Therefore, although the methods developed for the base metal can be applied to welds, it may be necessary to make certain corrections or adjustments to account for these additional factors. A defect tolerance analysis can help identify the critical defects that may be present in the weld and determine the appropriate level of inspection and testing required to ensure its integrity.

MATERIAL AND TENSILE TESTS

Chemical compositions for the API 5L X65 steel pipe, as provided by the supplier, are presented in **Table 1**. All specimens were extracted from a seamless pipe segment using electron discharge machining at pipe sections as shown in **figure 1**. The pipe had a wall thickness $t = 23.8$ mm and outside diameter $D_o = 1{,}219$ mm ($D_o/t = 51$).

TABLE 1

Chemical composition of X65 steel (wt. %)

Material	C	Mn	Si	Cr	Mo	Cu	Ni	P	S
X65	0.120	1.600	0.450	0.500	0.500	0.500	0.500	0.250	0.015

FIG. 1

Pipe of 1,219 mm external diameter and 23.80 mm thickness from which all specimens are extracted.

This geometry typifies the current trend of deep-water submarine pipelines made of high-grade steels. The notch orientation was machined parallel to the pipe rolling direction (L-C) as shown in **figure 2**. The first letter indicates the direction normal to crack plane and the second letter indicates the crack growth direction, with C = circumferential direction, L = longitudinal direction, and R = radial direction. The orientation circled in red (**fig. 2**) represents the orientation used in this study that was machined out from sections as shown in **figure 1**. Mechanical properties (see **Table 2**) and stress-strain behavior of X65 steel are obtained according to BS EN ISO 6892, *Metallic Materials. Tensile Testing - Method of Test at Room Temperature*,[21] using standard round specimens (diameter of 10 mm and a gage length of 60 mm) at room temperature and −120°C (fig. C.4 in the Supplementary Information shows the geometry).

Similarly, flat tensile specimens with 3 mm thickness and gage length of 90 mm (see fig. C.3 in the Supplementary Information) were used to obtain the engineering stress-strain data at room temperature and −120°C. These data were then processed to convert engineering stress-strain to true plastic stress-strain (see **fig. 3**), which shows yield strength increasing with decreasing temperature.

In our study on the mechanical properties of materials for an oil and gas pipeline, the decision to conduct testing at −120°C was based on a careful consideration of factors related to both safety and environmental conditions. The choice of this specific temperature is rooted in the following reasons.

Extreme Operating Conditions

The oil and gas pipeline in question traverses through regions characterized by extreme cold climates, including Arctic environments where temperatures can drop to exceptionally low values. Although temperatures of

FIG. 2

Sample orientations within a cylindrical section of material.[16]

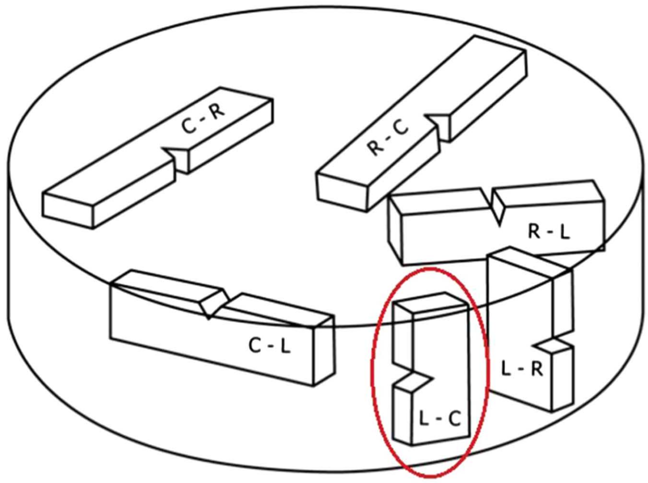

TABLE 2

Mechanical properties of API 5L X65 steel at room and low temperatures

$\sigma_{0.2\%YS}$, MPa	σ_{UTS}, MPa	E, MPa	ν	Elongation, %	σ_{UTS}/σ_{YS}
		Room temperature (23°C)			
446	579	207,000	0.3	27.3	1.3
		Low temperature (−120°C)			
593	746	213,000	0.3	32.8	1.3

FIG. 3

True stress-plastic strain curves for API 5L X65 pipeline steel at 23°C and −120°C.

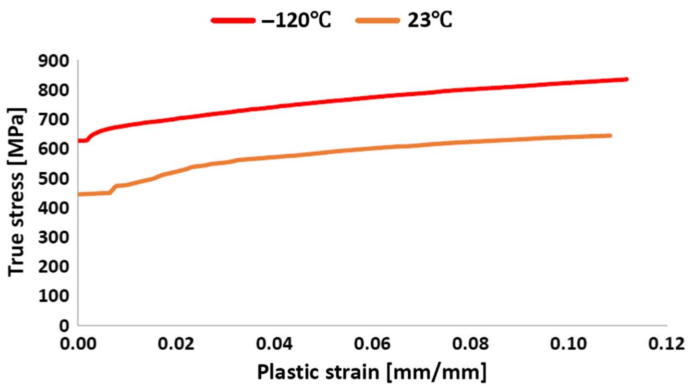

−60°C/70°C might indeed represent the Arctic minimum, testing at −120°C provides an additional margin of safety, considering potential fluctuations and unforeseen circumstances. It ensures that the material can withstand even the harshest conditions, providing a more comprehensive assessment of their performance.

Worst-Case Scenario Considerations

By selecting −120°C, we are aiming to simulate a worst-case scenario where the material face not only the minimum Arctic temperatures but also potential deviations or anomalies in the operating conditions. This approach is especially critical in ensuring the pipeline's resilience and integrity under extreme circumstances.

Material Performance Beyond Minimum Requirements

Although −60°C/70°C might indeed be representative of typical Arctic minimum temperatures, opting for −120°C reflects a commitment to ensuring that the materials not only meet but exceed minimum performance requirements. This level of rigor is particularly important in critical infrastructure like oil and gas pipelines, where safety and reliability are paramount.

FRACTURE TOUGHNESS TEST

Fracture toughness tests for three-point SENB and pin-loaded SENT specimens were conducted for the API 5L X65 steel following ISO 12135, *Metallic Materials: Unified Method of Test for the Determination of Quasistatic Fracture Toughness*,[22] and BS 8571, *Method of Test for Determination of Fracture Toughness in Metallic Materials Using Single Edge Notched Tension (SENT) Specimens*,[16] respectively. The dimensions of the respective configurations tested are shown in **Table 3** and the geometries are shown in figures C.1 and C.2 in the Supplementary Information. Localized cooling can be applied to SENT specimens clamped and loaded vertically, using a flow of liquid nitrogen vapor within insulation around the notch location. This method is effective for modest cooling, down to around −60°C, below which it can be difficult to establish a sufficiently constant and stable temperature for the duration of the soak time. Therefore, the pin-loaded SENT specimen was selected for this test to be able to test at the lower temperature of −120°C in an environmental chamber without the need for insulation. The SENB and SENT specimens were tested at 23°C and −120°C (using liquid nitrogen as shown in **fig. 4**) in an environmental chamber using the single specimen method, with setups shown in **figure 5*A*** and **5*B***, respectively. The specimens were tested to maximum/fracture load, then unloaded, and the corresponding fracture toughness, J_0, was recorded. The choice of dimensions and configurations of the specimens were based on numerical analysis conducted to ascertain suitability of slenderness for testing. The crack depth-to-width ratios, $a_0/W = 0.1$, 0.3, and 0.5, were achieved using fatigue precracking. In total, 36 specimens were tested, with 3 repetitions per crack configuration. Force and crack mouth opening displacements (CMOD) were obtained from load cell and displacement clip gages at a crosshead rate of 0.5 mm/min for SENB and 1 mm/min for SENT.

The CMOD was calculated from displacement measurements through equation (1)[16,22]:

$$CMOD = V_{p1} - \frac{Z_1}{Z_2 - Z_1}(V_{p2} - V_{p1}) \tag{1}$$

where V_{p1} and V_{p2} are the plastic parts of the clip gage displacements of knife heights Z_1 and Z_2, respectively.

The J value (J_0) was calculated at each assessment point based on equations given in BS 8571:2018[16] and ISO 12135[22]:

TABLE 3
Fracture specimen dimensions

B, mm	W, mm	a, mm	a/W
	Pin-loaded SENT		
15	30	3	0.1
15	30	9	0.3
15	30	15	0.5
	Three-point SENB		
15	30	3	0.1
15	30	9	0.3
15	30	15	0.5

FIG. 4

Test apparatus used for SENB and SENT low-temperature fracture tests.

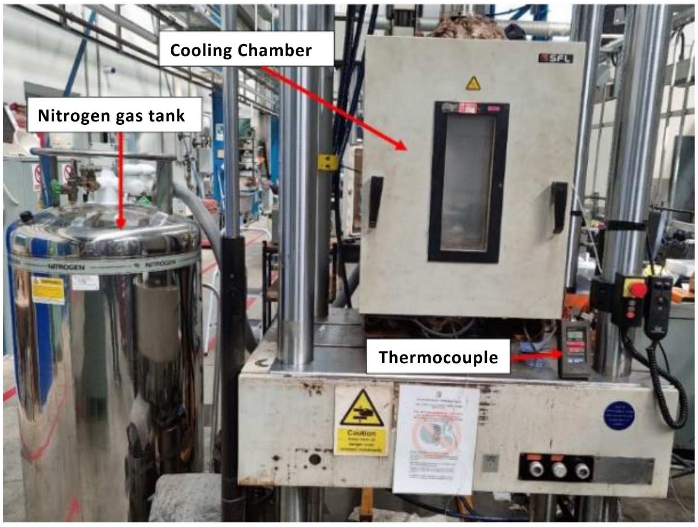

$$J = J_{el} + J_{pl} = \frac{K^2}{E'} + \frac{\eta_p U_p}{B b_0} \tag{2}$$

where J_{el} and J_{pl} are the elastic and plastic components of J, respectively; K is the elastic stress intensity factor (SIF) determined from the force acting on the specimen at the start of unloading; E' is the longitudinal elastic modulus in-plane strain; η_p is a dimensionless function of geometry; U_p is the area under the plastic part of the load versus CMOD curve; B is the specimen thickness; and b_0 is the crack ligament length $(W - a)$. The values of K and η_p were obtained for the calculation of J (J_0) based on the respective equations provided in BS 8571:2018[16] and ISO 12135,[22] which were incorporated in the software used for the testing.

CONSTRAINT ANALYSIS FOR SENB AND SENT SPECIMENS

To apply constraint-sensitive defect assessment procedures in BS 7910 Annex N,[4] the fracture toughness (J_0 values) obtained from experiments for various crack configurations were reindexed in terms of the elastic T stress ($\beta_T L_r$). The procedure described in BS 7910 Annex N[4] was used to calculate the relative collapse load, L_r, and T stress in this study as summarized in **figure 6**.

Structural integrity assessment of engineering components is assessed in terms of parameters which measure the proximity to either plastic collapse or brittle fracture within linear-elastic fracture mechanics (LEFM). The applied load, P, is compared with the plastic collapse load, P_L, through a parameter, L_r. This can also be defined in terms of the reference stress (σ_{ref}) that characterizes the distribution of stress in the vicinity of a flaw and yield strength (σ_y), as defined in BS 7910[4]:

$$L_r = \frac{\sigma_{ref}}{\sigma_y} = \frac{P}{P_L} \left(= \frac{applied\ load}{limit\ load} \right) \tag{3}$$

where:

L_r is the collapse ratio on the horizontal axis of a FAD,

σ_y is the lower-bound 0.2 % offset yield strength (MPa), and

σ_{ref} is the reference stress (MPa).

FIG. 5

Fracture test setup at −120°C using a cooling chamber suitable for liquefied nitrogen gas using a single-point specimen method: (*A*) SENB and (*B*) pin-loaded SENT.

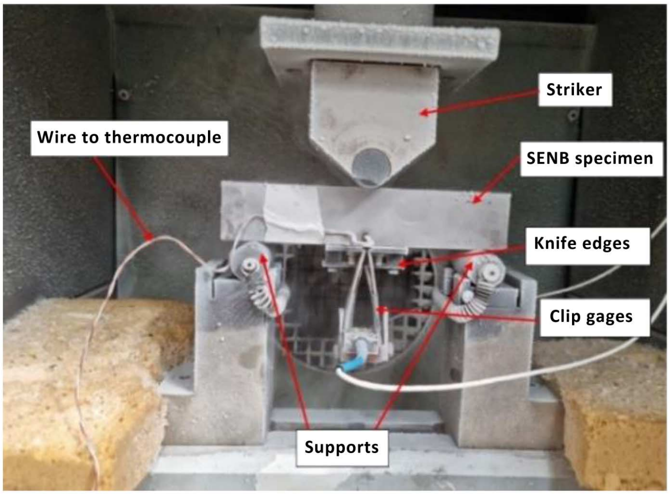

(*A*)

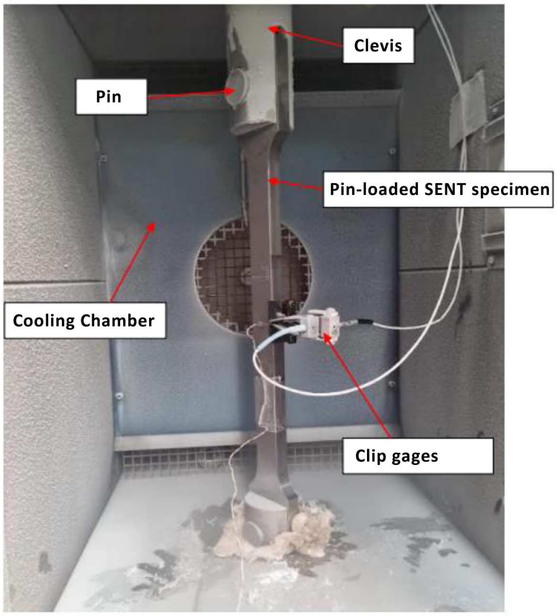

(*B*)

When $L_r = 1$, then σ_{ref} is equal to σ_y. The limit load in FAD is required for the calculation of σ_{ref}. For instance, the reference stress that characterizes the increase in stress in the vicinity of a flaw for a through-thickness flaw in plates under combined tension and bending is calculated as given in Annex P of BS 7910[4] and shown in equation (4). Please refer to Annex P of BS 7910 for the calculation of reference stress for different geometries.

$$\sigma_{ref} = \frac{P_b + (P_b^2 + 9P_m^2)^{0.5}}{3\{1 - (\frac{2a}{W})\}} \quad (4)$$

where:

P_b is the primary bending stress (MPa),

FIG. 6

Constraint-based procedure used in this study. SSY = small-scale yielding.

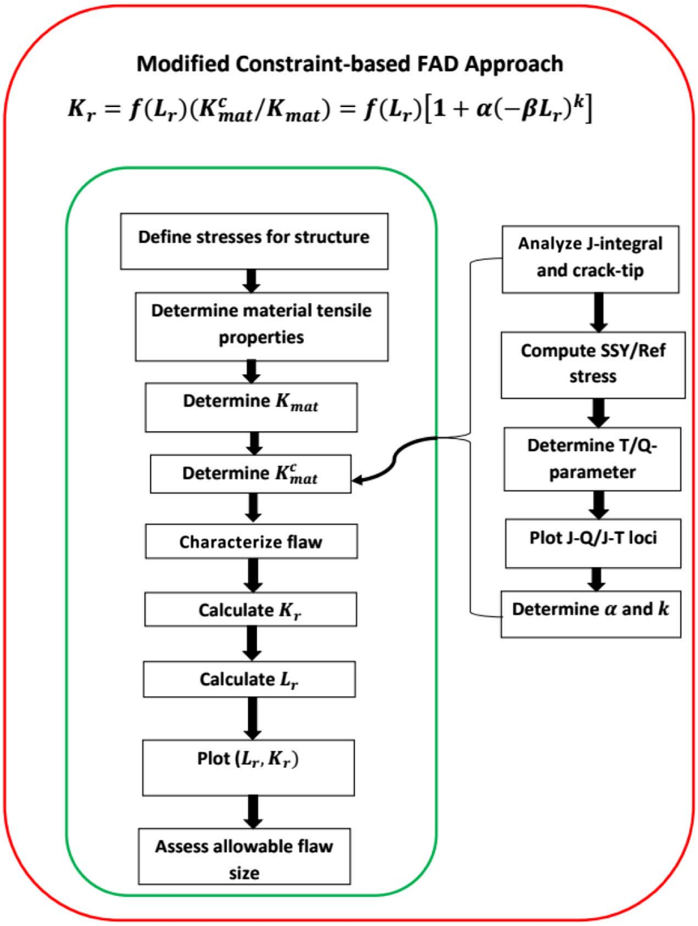

P_m is the primary membrane stress (MPa),
a is half crack length for through-thickness flaw (mm), and
W is the plate width (mm).

Primary stresses arise in a structure due to mechanical loads and contribute to plastic collapse. The primary bending stress, P_b, is the local average stress across the thickness of a component/structure developed due to mechanical loads and includes the effect of discontinuities. Thus, when a component is subjected to a bending moment, it experiences internal forces that result in both tensile and compressive stresses across its cross section. The primary membrane stress, P_m, on the other hand, is the average stress across the thickness of a component or structure developed due to the mechanical loads.[4]

Similarly, the possibility of fracture under LEFM is quantified by the ratio of the applied SIF, K_I, to an experimentally measured material toughness, K_{mat}. In simpler terms, it means that the potential for fracture is assessed by comparing the stress applied to the material with its inherent ability to resist fracture, as determined by experimental measurements of material toughness. To use the notation of J-based fracture mechanics (elastic-plastic materials), the ordinate of the FAD is written in terms of the fracture toughness J_{mat} and the elastic component of the driving force $J_{elastic}$:

$$K_r = \frac{K_I}{K_{mat}} = \sqrt{\frac{J_{elastic}}{J_{mat}}} \tag{5}$$

where:

K_I is the applied SIF, and

K_{mat} and J_{mat} are measures of the material's fracture toughness.

BS 7910[4] provides a method for defect assessment that may be related to J and crack opening displacement approaches. BS 7910,[4] however, has conservatisms introduced in approximate failure assessment curves (FACs) and also in the use of fracture toughness data from deeply cracked bend specimens. Improvement in the methods used to reduce this conservatism by consideration of constraint effects has been the subject of ongoing research.

Flaws in real structural components are typically surface cracks (low constraint) that contrast significantly with the deeply cracked specimens of standardized fracture toughness testing. Therefore, Ainsworth[23] and Ainsworth and O'Dowd[24] incorporated constraint effects through modification of the FAC by quantifying constraint through the normalized structural parameter, β, and a function of material behavior through the parameters α and k. The normalized constraint parameter, β, can be expressed by either elastic T stress or Q parameter, using the following:

$$\beta_T = \frac{T}{L_r \sigma_y} \tag{6}$$

$$\beta_Q = \frac{Q}{L_r} \tag{7}$$

β_T and β_Q are the normalized structural constraint parameters, which both depend on the geometry, crack size, and loading configurations. Negative values of β_T or β_Q correspond to low constraint, whereas positive values, as in deeply cracked bend geometries, correspond to high constraint.

The limit load required for calculation of L_r for SENB specimens is given by the following[5]:

$$P_L = \left(\frac{W^2 B \sigma_Y}{S}\right) f_L \tag{8}$$

where:

W, B, and S are specimen width, thickness, and span, respectively,

σ_Y is offset yield strength, and

f_L is the Von Mises yield factor.

For plane strain conditions, the Von Mises yield factor, f_L, for SENB is given by the following[5]:

$$f_L = \frac{2}{\sqrt{3}}\left(1.12 + 1.13\left(\frac{a}{W}\right) - 3.194\left(\frac{a}{W}\right)^2\left(1 - \frac{a}{W}\right)^2\right) for \left(0 \leq \frac{a}{W} \leq 0.18\right) \tag{9}$$

$$f_L = \frac{2.44}{\sqrt{3}}\left(1 - \frac{a}{W}\right)^2 for \left(0.18 \leq \frac{a}{W} \leq 1\right) \tag{10}$$

Negative values of β_T (or β_Q) are associated with a loss of crack tip constraint and an increase in fracture toughness. Because β_T depends only on specimen geometry, flaw size, and loading type (not magnitude), this can be defined by simple polynomial expressions as per Annex N of BS 7910 for various geometries.[4] The normalized constraint parameters, β_T for three-point SENB and SENT specimens for $0 \leq \frac{a}{W} \leq 0.8$, are summarized in equations (11) and (12), respectively:

$$\textbf{SENB}: \beta_T = -0.7887 - 0.1795\left(\frac{a}{W}\right) + 32.9014\left(\frac{a}{W}\right)^2 - 153.45\left(\frac{a}{W}\right)^3 + 316.11\left(\frac{a}{W}\right)^4 - 308.47\left(\frac{a}{W}\right)^5 + 115.18\left(\frac{a}{W}\right)^6 \quad (11)$$

$$\textbf{SENT}: \beta_T = -0.5889 - 0.0128\left(\frac{a}{W}\right) + 0.5512\left(\frac{a}{W}\right)^2 + 4.651\left(\frac{a}{W}\right)^3 - 4.6703\left(\frac{a}{W}\right)^4 \quad (12)$$

The plane strain Von Mises limit load solution for pin-loaded SENT specimens[5] is as follows:

$$P_L = WB\sigma_Y f_L \quad (13)$$

where

$$f_L = \left(\gamma/1.702\right)\left(1 - \left(\frac{a}{W}\right) - 1.232\left(\frac{a}{W}\right)^2 + \left(\frac{a}{W}\right)^3\right) for \left(0 \leq \frac{a}{W} \leq 0.545\right)$$

$$\gamma = 3.404/\sqrt{3} \quad (14)$$

MODIFICATION OF FAD

The combination of standard approach in BS 7910 Clause 7 and Annex N, "Allowance for Constraint Effects," is an attempt to characterize constraint quantitatively using a stress-based two-parameter fracture mechanics approach, through the elastic T stress or Q parameter.[4]

Essentially, Annex N of BS 7910[4] allows the user to quantify the constraint conditions associated with the structure being assessed and the small-scale specimens used to assess it, typically using either the elastic T stress or the Q parameter. Because the T stress requires only elastic calculations, it is used for the analyses in this study. It should be noted that the use of the elastic-plastic Q parameter gives very similar results to the linear-elastic T stress when plasticity is not widespread ($L_r < 1$).

A FAD represents a simple geometry-dependent failure locus (FAC), defined by the fracture ratio, K_r as a function of the applied load ratio, L_r[4]:

$$K_r = f\left(L_r\right) \quad (15)$$

By evaluating these two parameters using equations (3) and (5), failure could be avoided if the point (K_r, L_r) lies within the FAD,[24,25] as shown in **figure 7**.

To conduct a fracture assessment, both brittle and plastic collapse parameters are implemented in the FAD. This is an essential tool to assess the integrity of components or structures containing crack-like flaws. Both failure modes (brittle and ductile tearing) should be considered for fracture evaluation (structural integrity assessment). Note that the FACs are independent of the geometry and material strain-hardening properties.[24]

To examine the constraint effect, it is essential to have a measure of not only the structural constraint parameter but also the dependence of the material toughness on constraint. A constraint-dependent fracture toughness K_{mat}^c is dependent on βL_r and/or Q by the following[24]:

$$K_{mat}^C = \left\{ \begin{array}{c} K_{mat};\ \beta L_r, Q \geq 0 \\ K_{mat}[1 + \alpha(-\beta L_r)^k];\ \beta L_r < 0 \\ K_{mat}[1 + \alpha(-Q)^k];\ Q < 0 \end{array} \right\} \quad (16)$$

FIG. 7
FAD.[25]

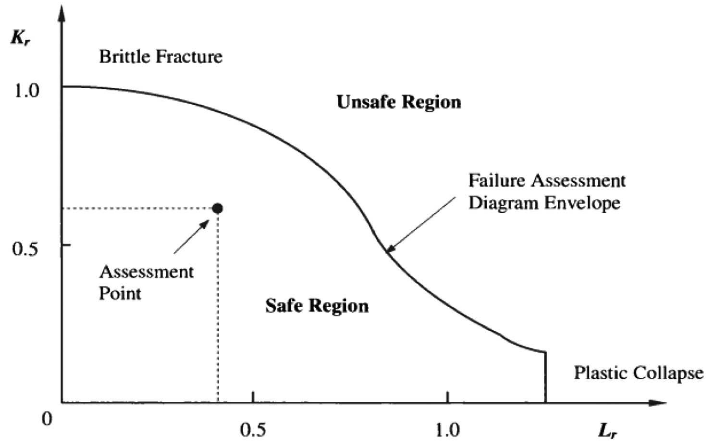

where α and k are constants that define the sensitivity of toughness to constraint variation for the material and temperature of interest. Sherry et al.[26] noted that α and k (a brief description of the determination of α and k for this study is given in Appendix A in the Supplementary Information) depend on fracture mechanisms, with ductile fracture initiation toughness generally exhibiting a lower sensitivity to constraint than brittle fracture toughness.

Two modifications to the constraint-based FAD approach are provided in BS 7910 Annex N[4] to account for constraint effects. First, the material toughness used to define K_r is set equal to K^c_{mat} rather than K_{mat}. In this way, the FAC remains unchanged from equation (15). However, because K^c_{mat} is a function of constraint and hence applied load, the loading curve becomes a nonlinear function of L_r. Instead, a modified FAD may be obtained by constructing the FAC using the relationship[24]:

$$K_r = f(L_r)\left(\frac{K^c_{mat}}{K_{mat}}\right) \tag{17}$$

Substituting equation (16) for $\beta L_r < 0$ into equation (17), the definitions of K_r and L_r remain unchanged and the FAC is modified for constraint according to the expression:

$$K_r = f(L_r)[1 + \alpha(-\beta L_r)^k] \tag{18}$$

where, in general, β is defined either in terms of T ($\beta_T L_r = T/\sigma_y$) or Q ($\beta_Q L_r = Q$).

This method of constraint-based fracture assessment involves the modification of the FAD but retains the definition of K_r given by equation (5). In other words, the fracture toughness obtained from the geometry with high crack tip constraint remains unchanged, but the FAC is modified by low constraint factors. Several authors, including but not limited to those in the reference list,[27–32] have shown that constraint-modified FAD can be used for a reduction in structural integrity conservatism.

There are several procedures that exist for the treatment of constraint loss such as the BS 7910,[4] R6,[5] and API 579/ASME[6] based on the work of Ainsworth and O'Dowd.[24] The procedure from BS 7910[4] was adopted in this paper for the construction of the FAD and is summarized as follows (see also **fig. 6**):

I. Measure the high-constraint fracture toughness K_{mat} using standard deeply cracked bend fracture specimens.
II. Evaluate the standard BS 7910 parameters K_r and L_r for the defective component.

III. Perform a FAD assessment using the standard FAC, $K_r = f(L_r)$.
IV. Evaluate the structural constraint parameters, β, for the defective component. In this paper, the elastic constraint parameter, $\beta_T = T/L_r\sigma_y$ is used, where T is the T stress.
V. Using a range of test specimen geometries and cracked sizes (here, SENT and shallow-cracked SENB), and hence a range of constraint levels, β, measure the low constraint toughness K^c_{mat}.
VI. Fit the data from step V with a function of the form, $K^c_{mat} = K_{mat}[1 + \alpha(-\beta L_r)^k]$.
VII. Construct a constraint-modified FAD using the FAC $f(L_r)[1 + \alpha(-\beta L_r)^k]$ and compare the assessment point (K_r, L_r) for the defective component with this modified curve.

These procedures were performed in CrackWISE software[20] to produce the FADs illustrated in the next section, which show the increased margin against fracture which are possible with constraint-based methods.

Results and Discussions

Figures 8, 9, C.5, and C.6 (see Supplementary Information for figs. C.5 and C.6) illustrate the relationship between crack depth, a/W, and the value of J at fracture (J_0) for the SENB and SENT specimens at −120°C and 23°C

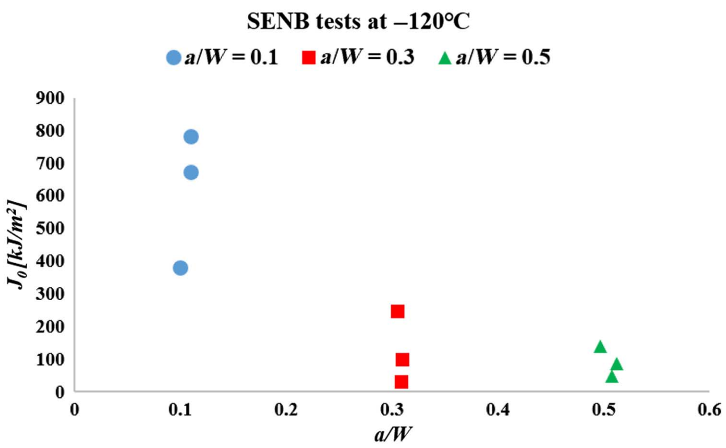

FIG. 8 Relationship between fracture toughness and crack depth for SENB at −120°C (cleavage fracture).

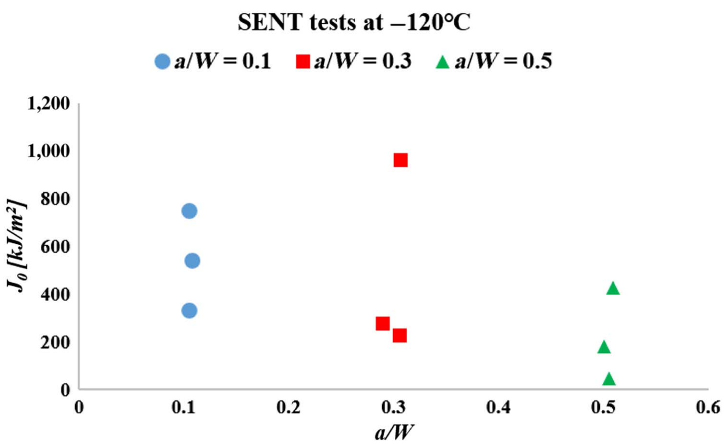

FIG. 9 Relationship between fracture toughness and crack depth for SENT at −120°C (cleavage fracture).

(cleavage and ductile fracture toughness). The observed increase in J_0 under low constraint conditions ($a/W = 0.1$) for most specimens suggests a trend that is consistent with the behavior expected under certain fracture mechanics conditions. However, the anomaly presented by the SENT specimen in figure C.6, which shows rather awkward low toughness at $a/W = 0.1$, requires a more detailed examination to understand the deviation from the expected trend. The material's response to crack propagation can vary based on factors such as microstructure, material composition, and heat treatment. Different specimens may exhibit distinct material behaviors under low constraint conditions. It is possible that the pipe section from which the SENT specimen was machined out had specific characteristics that resulted in lower toughness under these conditions. Furthermore, the microstructure of the material, including the presence of inclusions, grain boundaries, or other defects, can affect the fracture toughness. The SENT specimen may have a microstructure that is more sensitive to low constraint conditions. Last but not the least, experimental conditions, such as specimen preparation, loading rates and testing environment, can influence the fracture behavior. It is essential to ensure that the experimental setup for the fracture testing is consistent to eliminate potential experimental inaccuracies. There was an increase in fracture toughness by a factor of between 2 and 6 between the deeply cracked and shallow-notched SENB specimens at low (−120°C) temperature. These figures with the results in Tables B.1 and B.2 (Supplementary Information) show that majority of the shallow-cracked specimens ($a/W = 0.1$) at low (−120°C) temperature failed after undergoing more than 0.2 mm of ductile tearing. The fracture test results are presented in Appendix B in Supplementary Information.

Figures C.6–C.10 (Supplementary Information) illustrate the relationship between fracture toughness, J_0, and the amount of ductile tearing, Δa, for all experiments ($a/W = 0.1$, 0.3, and 0.5 at −120°C and 23°C, for SENB and SENT). The increasing value of fracture toughness was observed to be highly dependent on the amount of ductile tearing, Δa, which in turn depended on the initial crack depth, a/W. In the low temperature (−120°C) tests, there was failure after most of the $a/W = 0.1$ specimens had more than 0.2 mm ductile tearing. No significant amount of stable tearing was observed in the $a/W = 0.3$ and 0.5 specimens due to the deep cracks. At room temperature (23°C), ductile tearing was observed in each case at the end of the test. The cleavage and ductile fracture toughness properties play a significant role in the constraint-modified FAD procedure. It involves comparing the applied loading conditions with the material's fracture toughness properties to determine the structural integrity. These two different fracture toughness measures are important in the use of the constraint-modified FAD procedure and should be taken into account to define crack sizes and loadings where brittle or ductile fracture is likely to occur.

Figures 10, 11, C.11, and C.12 (Supplementary Information) show that shallow-notched bend specimens (those that have a loss of crack tip constraint and exhibit negative values of T), result in enhanced fracture

FIG. 10

Fracture toughness as a function of T stress for SENB at −120°C.

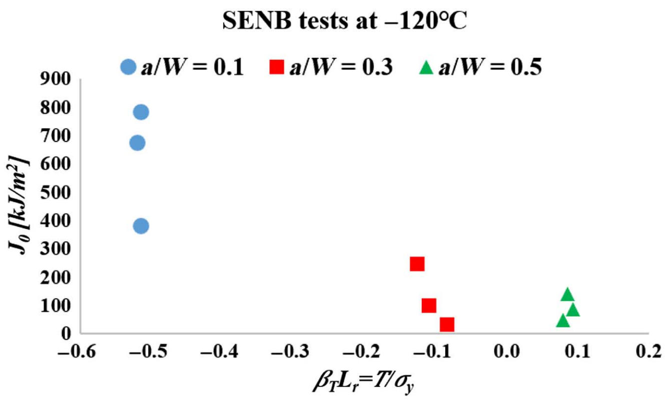

FIG. 11

Fracture toughness as a function of T stress for SENT at −120°C.

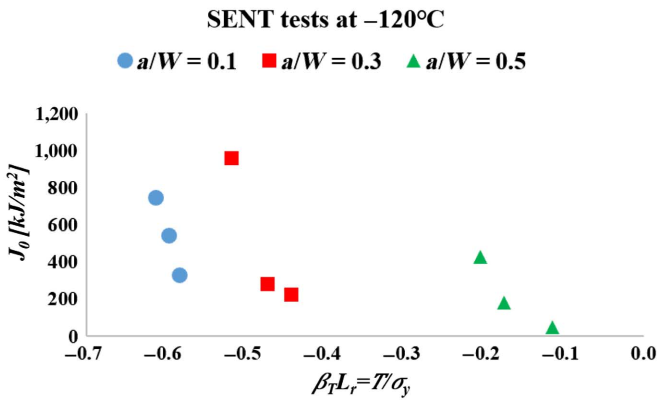

toughness at both low (−120°C) and room temperatures (typically, cleavage and ductile tearing mechanisms, respectively) compared to deeply cracked SENB geometries. Therefore, the resistance to fracture of the material in the presence of a crack is increased due to the low stresses near the crack tip. In contrast, deeply notched $a/W = 0.5$ feature positive values of T and a geometry-independent toughness associated with a highly constrained flow field. The geometry with a negative T stress indicates a low constraint level near the crack tip, whereas zero or positive T stress corresponds to a higher constraint level. This behavior is consistent with previous research carried out in references cited in this paper,[10,18,30,33,34] among others. Note in figure C.12 the low fracture toughness values for the low constraint SENT specimen ($a/W = 0.1$), which should normally not be the case, but this behavior could not be ascertained as to why this occurred during the test. Possible reasons for this inconsistency were given in the first paragraph of this "Results and Discussions" section when the anomaly in figure C.6 was discussed. However, it was observed that additional testing is recommended to determine a consistent relation between fracture toughness and constraint T/σ_Y because data scatter is high under high fracture toughness/low constraint conditions for SENB and all SENT crack configurations at −120°C.

Constraint-modified FADs are shown in **figures 12–15** for the SENB and SENT test specimens of a constraint-sensitive material based on experimental data. By combining the applied loading conditions, material properties, and dimensions of the defect, the structural integrity can be assessed and the likelihood of failure can be determined. The constraint-correction FADs are compared to those of the standard Option 1 approach in BS 7910. For Option 1 of BS 7910, a deep-notched specimen is typically used to populate the FAD, and this was adopted in this paper. The lower values of the toughness were adopted in all analyses. The deep cracked specimens are designed to simulate the behavior of cracked components or structures, allowing for safe but conservative assessment of their integrity. Therefore, there is merit in applying the experimental data from shallow-cracked SENB and SENT specimens to provide some form of refinement to the inherent conservatism in defect assessment procedures, particularly BS 7910.

The values of assessment points (L_r, K_r), primary bending, and primary membrane stresses are shown in **Tables 4** and **5**, respectively, for SENT and SENB specimens. These primary bending and primary membrane stresses were used alongside other mechanical properties obtained from the experiment to derive the FADs with constraint-correction factors in this study.

The lookup tables that provide values of α and k for use in equations (16) and (18) require knowledge of the Beremin parameter, m, and work-hardening exponent, n. **Figures 12–15** were established based on knowledge of the steel's yield and work-hardening behavior at the temperature of interest and the Beremin fracture model parameter, m.[26] A brief description of the Beremin parameter, m, and the material tensile properties is given in Appendix A in the Supplementary Information[35–37] of this paper. In cases where sufficient test data are

FIG. 12

FAD for a constraint-sensitive material, $m = 15$, SENB at $-120°C$.

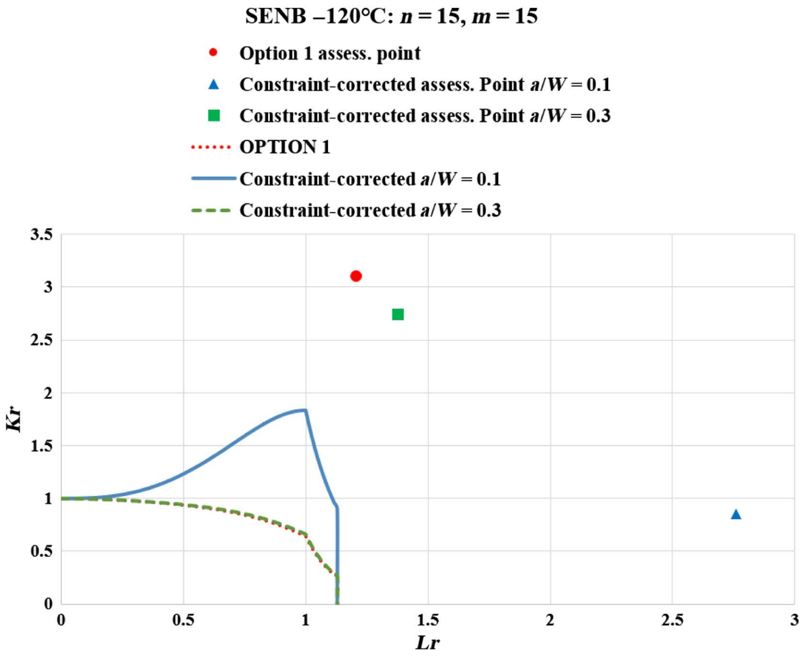

FIG. 13

FAD for a constraint-sensitive material, $m = 15$, SENT at $-120°C$.

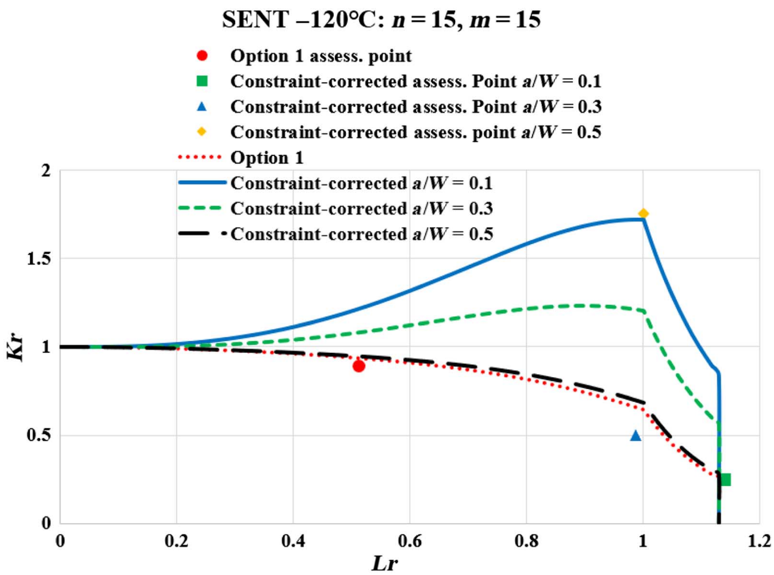

available, a value of m can be selected that gives the α and k values which provide the best fit to the data. Alternatively, m can be calibrated directly using test data from high and low constraint test specimens. This requires not only an extensive testing program but also detailed cracked-body large strain elastic-plastic finite element analysis of the test specimens as well as a suitable postprocessor to calculate the Weibull stress, σ_w.[26]

FIG. 14

FAD for a constraint-sensitive material, $m = 15$, SENB at 23°C.

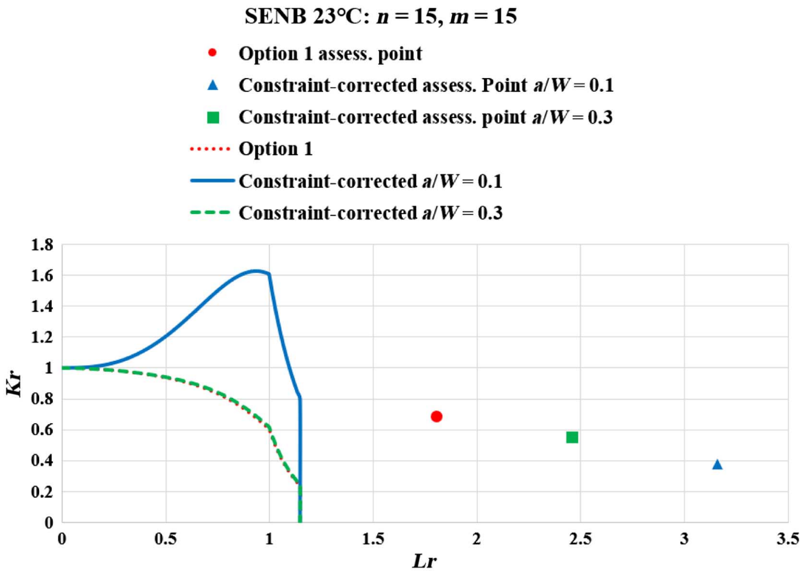

FIG. 15

FAD for a constraint-sensitive material, $m = 15$, SENT at 23°C.

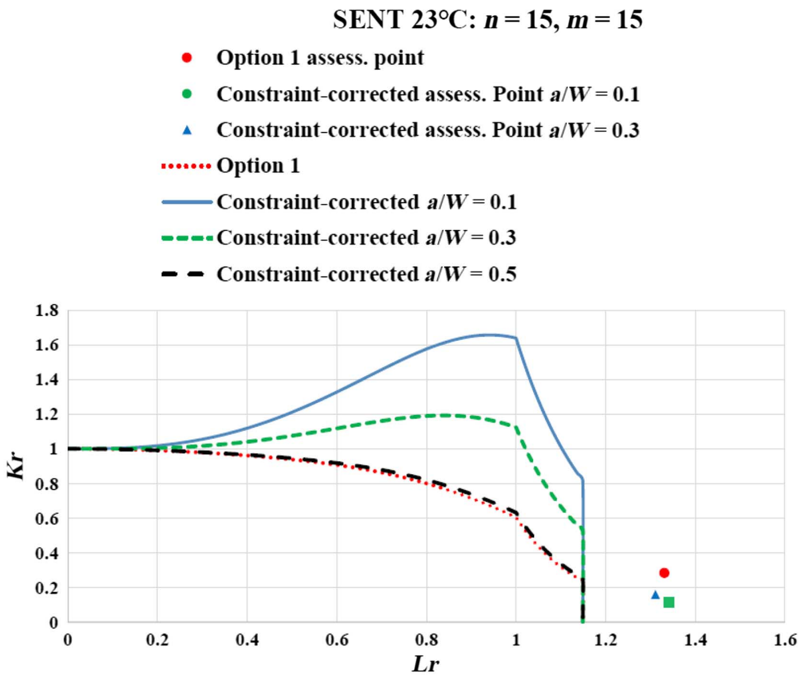

Therefore, the approach is analytically complex, labor intensive, and unsuitable for routine engineering application. Hence, it was convenient to select a value of m that gave α and k values which provided an increased margin in the FAD. Generally, lower values of m are insensitive to constraint and higher values of m are constraint-sensitive.

TABLE 4
Results of assessments and primary membrane stresses for SENT

a/W	L_r	K_r	P_m
	SENT at −120°C		
0.1	1.138505	0.251601	607.62
0.3	0.986967	0.499580	409.69
0.5	1.001315	1.754101	151.56
	SENT at 23°C		
0.1	1.341754	0.111957	538.58
0.3	1.311115	0.159502	409.33
0.5	1.331345	0.281218	296.89

TABLE 5
Results of assessment and primary bending stresses for SENB

a/W	L_r	K_r	P_b
	SENB at −120°C		
0.1	2.759765	0.851189	2,209.33
0.3	1.376905	2.744127	857.33
0.5	1.205171	3.104173	536.00
	SENB at 23°C		
0.1	3.160488	0.374988	1902.93
0.3	2.454837	0.552120	1,149.60
0.5	1.804096	0.686588	609.47

The work-hardening exponent, n (also employed in this paper), is a measure of a metal's ability to resist plastic deformation after it has yielded under stress. This is defined as the slope of the logarithmic relationship between stress and strain during plastic deformation phase of a tensile test. A high work-hardening exponent indicates that the material can withstand significant plastic deformation without fracturing or cracking. The value of the work-hardening exponent varies depending on the material being tested and the testing conditions. Details on the value of $n = 15$ and $m = 5$ and 15 used in this paper are given in Appendix A in the Supplementary Information.

At small fractions of the limit load ($L_r \rightarrow 0$), there is no effect of constraint or geometry, as failure occurs under essentially elastically controlled conditions. However, with increasing load, the constraint-enhanced toughness for shallow-cracked SENB configuration ($a/W = 0.1$) increases. For SENT ($a/W = 0.1$ and 0.3), an enlargement in the FAD is observed for both temperatures analyzed, with the largest adjustment at loads close to the limit load ($L_r = 1$); see **figures 12–15**. Therefore, there are significant advantages to be gained from this approach for applied loads with magnitudes close to the limit load (these stresses may be close to those at which engineering components are expected to operate). The analysis of the tests conducted on the SENB specimens at the low temperature generated assessment points that lie farther from the FAC, as all these specimens failed during the test. Noticeably, the high-constraint SENB specimen at low temperature (−120°C) in **figure 12** has K_r value of 3.1. Furthermore, it is observed that assessment points for the SENT at the same low temperature for the Option 1 and a/W= 0.3 cases have both the points within the FAC (indicating failure did not occur), but all the low temperature specimens fractured. This raises concerns about the specimens whose assessment points lie in the safe zone of the FACs, even though failure occurred. A possible explanation to this could be microstructural difference due to the low temperature; however, this was not verified as part of this research.

For the test conducted at room temperature, SENB specimens have assessment points that are almost in a straight line and lie further outside the FAC (all tests tested to maximum load, failure did not occur). The SENT, on the other hand, has assessment points outside the FAC that are almost clustered at the bottom end of the FAC.

Summary and Conclusions

Thirty-six fracture toughness tests have been carried out on API 5L X65 steel for SENT and SENB specimens at low (−120°C) and room temperatures. Crack lengths were 3, 9, and 15 mm, giving a_0/W ratios of 0.1, 0.3, and 0.5, respectively. A range of the experimental data for SENT and SENB has been analyzed where failure occurred by cleavage at temperatures of −120°C, where the material had a yield stress of 593 MPa. At room temperature, ductile tearing occurred when the specimens were loaded to maximum load without failure, where the material had a yield stress of 446 MPa. The strain-hardening characteristics were described by $n = 15$ based on the Beremin parameter, m, using the constraint-based FAD fracture assessment approach by varying crack depth (a/W) ratios.

It has been demonstrated that enhanced levels of toughness associated with loss of constraint occur in both ductile and cleavage-controlled fracture. These effects have major advantages for safety cases, which seek to demonstrate the integrity of engineering structures. Based on the constraint-based FAD methodology, fracture assessments were conducted with constraint-correction in the presence of cracks and compared to the conventional fracture assessment procedure in BS 7910 Option 1.

The following concluding remarks were drawn from this study:

- The decision to test specimens at −120°C is a deliberate but engineering decision made to provide a thorough and conservative assessment of the materials' mechanical properties. Although acknowledging that −60°C/70°C may be representative of Arctic minimum temperatures, the selection of −120°C ensures a robust evaluation that accounts for potential variations and extreme conditions, reinforcing the reliability and safety of the oil pipeline under investigation.
- The work demonstrated that a decrease in temperature leads to reduction in fracture toughness and therefore susceptibility to brittle failure for specimens tested at low temperature. This needs to be verified for real structures to ensure they are fit-for-service/purpose when operating in low temperature environments.
- SENT specimens exhibited larger fracture toughness (J values) than SENB specimens for both temperatures tested (except SENT at room temperature for the $a/W = 0.1$). This is because the SENT specimen is loaded in tension perpendicular to the notch, and this creates a mixed mode loading condition (both opening-mode I and shearing-mode III) stresses acting on the crack tip. The SENT specimen is designed to simulate more complex loading conditions that occur in real-world structures. For the SENB specimen, the notch is positioned on the tension side and the load is applied to the opposite side. This creates a pure mode I loading condition with opening stress acting on the notch tip. Therefore, low constraint (SENT and shallow-cracked bend) specimens showed higher values of fracture toughness than those associated with standard deeply cracked bend specimens at low (−120°C) and room temperatures.
- J values (J_0) were given as a function of a/W; this was translated into a J-T failure locus. Enhanced toughness is associated with shallow cracks, which develop negative values of T. The present work addresses the way in which advantage can be taken of this enhanced toughness in defect assessment procedures.
- The conventional fracture assessment method based on BS 7910 Option 1 FAD produces overconservative results if the constraint effect is not considered properly. Based on the work in this paper, the constraint-based FAD procedure may help to reduce excessively conservative predictions of failure. The enhanced toughness associated with loss of constraint implies that there is, in fact, an increased margin (as shown in the enlargement of the FAC for shallow-cracked SENT and SENB specimens).
- By understanding the degree of crack tip constraint in a structure, engineers can design and develop accurate fracture mechanics models and prediction methods specific to low temperature operation to minimize the risk of crack propagation and failure. Therefore, this research demonstrates the advantages of incorporating representative (enhanced) fracture toughness at low temperatures to support more realistic design and repair decisions.

ACKNOWLEDGMENTS

This work is supported by The Welding Institute, Ltd., National Structural Integrity Research Centre, Brunel University London, and Lloyd's Register Foundation as part of their PhD grant. Lloyd's Register Foundation helps to protect life and property by supporting engineering-related education, public engagement, and the application of research (http://www.lrfoundation.org.uk).

SUPPLEMENTARY INFORMATION

Appendixes for this paper are available at https://doi.org/10.6084/m9.figshare.25188575.

References

1. R. H. Dodds Jr., T. L. Anderson, and M. T. Kirk, "A Framework to Correlate a/W Ratio Effects on Elastic-Plastic Fracture Toughness (Jc)," *International Journal of Fracture* 48, no. 1 (March 1991): 1–22, https://doi.org/10.1007/BF00012499
2. S. Cicero, R. A. Ainsworth, and F. Gutiérrez-Solana, "Engineering Approaches for the Assessment of Low Constraint Fracture Conditions: A Critical Review," *Engineering Fracture Mechanics* 77, no. 8 (May 2010): 1360–1374, https://doi.org/10.1016/j.engfracmech.2010.02.026
3. Y. K. Kim, B. T. Oh, and J. H. Kim, "Effects of Crack Tip Constraint on the Fracture Toughness Assessment of 9% Ni Steel for Cryogenic Application in Liquefied Natural Gas Storage Tanks," *Materials* 13, no. 22 (November 2020): 5250, https://doi.org/10.3390/ma13225250
4. *Guide to Methods for Assessing the Acceptability of Flaws in Metallic Structures*, BS 7910:2019 (London: British Standards Institution, 2019).
5. *British Energy Generation Limited: Assessment of the Integrity of Structures Containing Defects*, R6 Revision 4 (London: EDF Energy UK, 2009).
6. *Fitness-for-Service*, API 579-1/ASME FFS-1 (New York: The American Society of American Engineers, 2021).
7. U. Zerbst, M. Schödel, S. Webster, and R. A. Ainsworth, *Fitness-for-Service Fracture Assessment of Structures Containing Cracks: A Workbook Based on the European SINTAP/FITNET Procedure*, 1st ed. (Amsterdam, the Netherlands: Elsevier, 2007).
8. S. Cravero and C. Ruggieri, "Estimation Procedure of *J*-Resistance Curves for SE(T) Fracture Specimens Using Unloading Compliance," *Engineering Fracture Mechanics* 74, no. 17 (November 2007): 2735–2757, https://doi.org/10.1016/j.engfracmech.2007.01.012
9. A. Neimitz and J. Galkiewicz, "Fracture Toughness of Structural Components: Influence of Constraint," *International Journal of Pressure Vessels and Piping* 83, no. 1 (January 2006): 42–54, https://doi.org/10.1016/j.ijpvp.2005.10.001
10. S. Cravero and C. Ruggieri, "Structural Integrity Analysis of Axially Cracked Pipelines Using Conventional and Constraint-Modified Failure Assessment Diagrams," *International Journal of Pressure Vessels and Piping* 83, no. 8 (August 2006): 607–617, https://doi.org/10.1016/j.ijpvp.2006.04.004
11. J. Xu, Z. L. Zhang, E. Østby, B. Nyhus, and D. B. Sun, "Constraint Effect on the Ductile Crack Growth Resistance of Circumferentially Cracked Pipes," *Engineering Fracture Mechanics* 77, no. 4 (March 2010): 671–684, https://doi.org/10.1016/j.engfracmech.2009.11.005
12. J. Xu, Z. L. Zhang, E. Østby, B. Nyhus, and D. B. Sun, "Effects of Crack Depth and Specimen Size on Ductile Crack Growth of SENT and SENB Specimens for Fracture Mechanics Evaluation of Pipeline Steels," *International Journal of Pressure Vessels and Piping* 86, no. 12 (Decenver 2009): 787–797, https://doi.org/10.1016/j.ijpvp.2009.12.004
13. B. Nyhus, M. L. Polanco, and O. Ørjasæther, "SENT Specimens an Alternative to SENB Specimens for Fracture Mechanics Testing of Pipelines," in *ASME 2003 22nd International Conference on Offshore Mechanics and Arctic Engineering* (New York: American Society of Mechanical Engineers, 2009), 259–266, https://doi.org/10.1115/OMAE2003-37370
14. J. Xu, X. M. Zhuo, P. P. Li, Y. Fan, and Z. Sun, "Constraint Effect on the Ductile Fracture Behavior of High-Strength Pipeline Steels," *Materials Science Forum* 850 (2016): 899–904, https://doi.org/10.4028/www.scientific.net/MSF.850.899
15. J. Xu and Y. Fan, "Effects of Temperature and Crack Tip Constraint on Cleavage Fracture Toughness in the Weld Thermal Simulated X80 Pipeline Steels," *Advanced Materials Research* 197–198 (2011): 1595–1598, https://doi.org/10.4028/www.scientific.net/AMR.197-198.1595
16. *Method of Test for Determination of Fracture Toughness in Metallic Materials Using Single Edge Notched Tension (SENT) Specimens*, BS 8571:2018-TC (London: British Standards Institution, 2018).
17. J. Kang, J. A. Gianetto, and W. R. Tyson, "Recent Development in Low-Constraint Fracture Toughness Testing for Structural Integrity Assessment of Pipelines," *Frontiers of Mechanical Engineering* 13, no. 4 (December 2018): 546–553, https://doi.org/10.1007/s11465-018-0501-2
18. C. Ruggieri, "Low Constraint Fracture Toughness Testing Using SE(T) and SE(B) Specimens," *International Journal of Pressure Vessels and Piping* 156 (September 2017): 23–39, https://doi.org/10.1016/j.ijpvp.2017.07.003
19. D. F. B. Sarzosa and C. Ruggieri, "A Numerical Investigation of Constraint Effects in Circumferentially Cracked Pipes and Fracture Specimens Including Ductile Tearing," *International Journal of Pressure Vessels and Piping* 120–121 (August–September 2014): 1–18, https://doi.org/10.1016/j.ijpvp.2014.03.005
20. TWI Global, "CrackWISE® Version 6.0 (CW6)," The Welding Institute, 2020, https://web.archive.org/web/20240204112255/https://www.twisoftware.com/software/integrity-management-software/crackwise/

21. *Metallic Materials. Tensile Testing - Method of Test at Room Temperature*, BS EN ISO 6892-1:2019-TC (London: British Standards Institute, 2019).
22. *Metallic Materials: Unified Method of Test for the Determination of Quasistatic Fracture Toughness*, ISO 12135:2021 (Genva, Switzerland: International Organization for Standardization, 2021).
23. R. A. Ainsworth, "A Constraint-Based Failure Assessment Diagram for Fracture Assessment," *International Journal of Pressure Vessels and Piping* 64, no. 3 (1995): 277–285, https://doi.org/10.1016/0308-0161(95)98949-7
24. R. A. Ainsworth and N. P. O'Dowd, "Constraint in the Failure Assessment Diagram Approach for Fracture Assessment," *Journal of Pressure Vessel Technology* 117, no. 3 (August 1995): 260–267, https://doi.org/10.1115/1.2842121
25. M. M. Hossain, "Simplified Design and Integrity Assessment of Pressure Components and Structures" (PhD diss., Memorial University, 2009).
26. A. H. Sherry, D. G. Hooton, D. W. Beardsmore, and D. P. G. Lidbury, "Material Constraint Parameters for the Assessment of Shallow Defects in Structural Components. Part II: Constraint-Based Assessment of Shallow Defects," *Engineering Fracture Mechanics* 72, no. 15 (October 2005): 2396–2415, https://doi.org/10.1016/j.engfracmech.2004.12.010
27. W. Y. Peng, H. J. Jin, and S. J. Wu, "Structural Integrity Analysis of Cracked Pressure Vessel Welds Using Conventional and Constraint-Modified Failure Assessment Diagrams," *Procedia Engineering* 130 (2015): 835–844, https://doi.org/10.1016/j.proeng.2015.12.204
28. R. A. Ainsworth, "Failure Assessment Diagrams for Use in R6 Assessments for Austenitic Components," *International Journal of Pressure Vessels and Piping* 65, no. 3 (1996): 303–309, https://doi.org/10.1016/0308-0161(94)00141-5
29. O. Bouledroua, M. Hadj Meliani, and G. Pluvinage, "Assessment of Pipe Defects Using a Constraint-Modified Failure Assessment Diagram," *Journal of Failure Analysis and Prevention* 17, no. 1 (February 2017): 144–153, https://doi.org/10.1007/s11668-016-0221-z
30. I. Hadley and A. Horn, "Treatment of Constraint in BS 7910:2013, ISO 27306 and DNVGL-RP-F108," *International Journal of Pressure Vessels and Piping* 169 (January 2019): 77–93, https://doi.org/10.1016/j.ijpvp.2018.11.015
31. C. Rodriguez, F. J. Belzunce, T. E. Garcia, and I. Peñuelas, "Constraint Dependence of the Fracture Toughness of Reduced Activation Ferritic-Martensitic Eurofer Steel Plates," *Engineering Fracture Mechanics* 103 (May 2013): 60–68, https://doi.org/10.1016/j.engfracmech.2012.05.003
32. D. H. Moon, J. Y. Park, and M. H. Kim, "Effects of the Crack Tip Constraint on the Fracture Assessment of an AI 5083-O Weldment for Low Temperature Applications," *Materials* 10, no. 7 (July 2017): 815, https://doi.org/10.3390/ma10070815
33. I. Hadley and S. A. Karger, *Effect of Crack Tip Constraint on Fracture Toughness of A533B Steel and Validation of the Sintap Constraint, TWI Report Number: SINTAP/TWI/012* (London: The Welding Institute, 1999).
34. I. MacLennan and J. W. Hancock, "Constraint-Based Failure Assessment Diagrams," *International Journal of Pressure Vessels and Piping* 64, no. 3 (1995): 287–298, https://doi.org/10.1016/0308-0161(95)98950-B
35. F. M. Beremin, A. Pineau, F. Mudry, J. C. Devaux, Y. D'Escatha, and P. Ledermann, "A Local Criterion for Cleavage Fracture of a Nuclear Pressure Vessel Steel," *Metallurgical Transactions A* 14, no. 11 (November 1983): 2277–2287, https://doi.org/10.1007/BF02663302
36. X. Gao, C. Ruggieri, and R. H. Dodds Jr., "Calibration of Weibull Stress Parameters Using Fracture Toughness Data," *International Journal of Fracture* 92, no. 2 (July 1998): 175–200, https://doi.org/10.1023/A:1007521530191
37. A. H. Sherry, M. A. Wilkes, D. W. Beardsmore, and D. P. G. Lidbury, "Material Constraint Parameters for the Assessment of Shallow Defects in Structural Components – Part I: Parameter Solutions," *Engineering Fracture Mechanics* 72, no. 15 (October 2005): 2373–2395, https://doi.org/10.1016/j.engfracmech.2004.12.009